Phys. Status Solidi A **209,** No. 9, 1619–1630 (2012) / **DOI** 10.1002/pssa.201200576

physica status solidi a
www.pss-a.com
applications and materials science

Part of Topical Section on
Fundamentals and Applications of Diamond

Feature Article

Diamond nanophotonics and applications in quantum science and technology

B. J. M. Hausmann*[,1], J. T. Choy[1], T. M. Babinec[1], B. J. Shields[2], I. Bulu[1], M. D. Lukin[2], and Marko Lončar*[,1]

[1] School of Engineering and Applied Sciences, Harvard University, Cambridge, MA 02138, USA
[2] Department of Physics, Harvard University, Cambridge, MA 02138, USA

Received 14 August 2012, revised 22 August 2012, accepted 23 August 2012
Published online 17 September 2012

Keywords diamond photonics, NV center

* Corresponding authors: e-mail hausmann@seas.harvard.edu, loncar@seas.harvard.edu, Phone: +1 617 495 579, Fax: +1 617 496 6404, Web: http://nano-optics.seas.harvard.edu

Diamond nanophotonics have evolved tremendously from the study of color centers in bulk single crystals and nanocrystals to their characterization in nanostructured environments. This development was facilitated by the ability to generate monolithic, sophisticated nanodevices in high quality single crystal diamond. Here, we present some recent contributions to the field of diamond nanophotonics: increase in single photon collection from nitrogen vacancy (NV) centers embedded in diamond nanowires, broadband spontaneous emission enhancement of single NV centers in plasmonic resonators, and coupling of single NV centers to planar resonators on-chip.

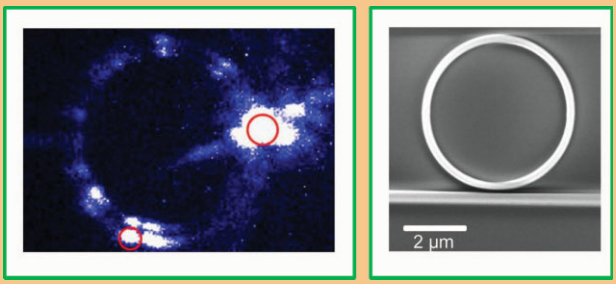

1 Introduction Researchers have long been attracted to diamond for its many unique properties. For example, diamond's large refractive index ($n = 2.4$) and the presence of color centers, such as the silicon vacancy (SiV) and nitrogen vacancy (NV) centers [3], that can be addressed individually using optical excitations, are of particular interest to the field of quantum optics and photonics. Notably, the negatively charged NV center has been in the focus of diamond photonics research for more than 50 years [3] due to its stability, long electron-spin coherence time, and optical read-out capabilities. The NV center is formed by replacing one carbon atom in the diamond lattice by a nitrogen atom, and removing one adjacent carbon atom such that the NV center's axis is along the [111] direction (Fig. 1a). NV centers can be introduced either during the diamond's growth or after the diamond has formed, using ion implantation. The electronic levels of the negatively charged NV center, sketched in Fig. 1b, consist of triplet ground (^{3}A) and excited (^{3}E) states that are separated by 1.95 eV corresponding to 637 nm. The triplet ground state of the NV center is split by 2.87 GHz between the $m_s = 0$ and $m_s = \pm 1$ states [4]. A selective coupling between the excited states and the long-lived metastable singlet state (^{1}A$_1$), dependent on the initial ground state population, enables state-dependent fluorescence and spin-readout. The NV center's emission spectrum can be obtained using green excitation and consists of a zero-phonon line (ZPL) at 637 nm, a pure photon transition, and a broad phonon sideband (PSB) from 637 nm to around 800 nm that originates from phonon-assisted transitions. The electron-phonon coupling for an NV center is strong so that most of the spontaneous emission occurs into the PSB. Figure 1c shows the NV center's spectrum in a bulk diamond both at room and low temperature. At low temperature, the phonon-assisted transitions around the ZPL are suppressed and the ZPL becomes much more visible. The ZPL emission can be further increased using optical resonators as discussed below.

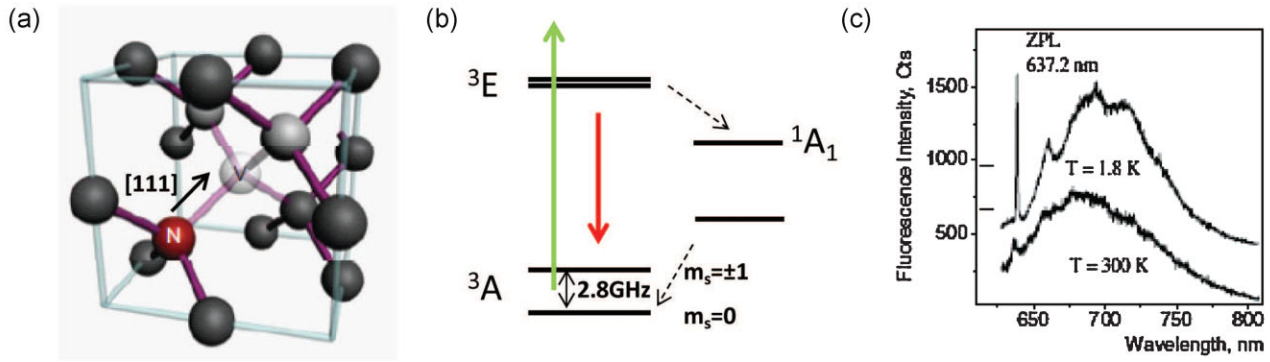

Figure 1 (online color at: www.pss-a.com) (a) Schematic of an NV center in the diamond carbon lattice. (b) Electronic level scheme of the negatively charged NV center, and (c) spectra of the NV center emission both at room and low temperature. (a and c) adapted from [1, 2], respectively, with courtesy of Balasubramanian and Jelezko.

As a stable single photon source, at both low and room temperatures [5], with optically detected magnetic resonance, the NV center is very attractive for applications [6] in magnetometry [7, 8] and quantum information science and technology [9, 10] and in particular for the realization of scalable quantum networks [11, 12]. These and other applications, however, depend crucially on the efficiency with which information can be exchanged between the NV center's electron spin (a "stationary" qubit in the context of quantum computation) and a photon (a "flying" qubit). Therefore, there has been great interest in increasing the photon–NV center interaction using diamond-based optical nanostructures. While quantum science and technology has been the main driving force behind recent interest in diamond nanophotonics, such platform would have many applications that go well beyond the quantum realm. For example, diamond's transparency over a wide wavelength range and large third-order nonlinearity are of great interest for the implementation of frequency combs. Furthermore, diamond's wide bandgap (5.5 eV), very large phonon energy (165 meV compared to 65 meV in Si), and excellent thermal properties are suitable for integrated, high-power Raman lasers [13, 14].

Birgit Hausmann is a PhD candidate in Applied Physics at Harvard University and is a recipient of the Harvard Quantum Optics Center fellowship. She received her Diploma in Physics from the Technical University of Munich, Germany, in 2009. During her studies, she received the LAOTSE fellowship to study at the Nanyang Technological University, Singapore. Her research focuses on nanophotonics, and in particular nanoscale resonators as well as single photon sources based on diamond.

Marko Lončar is Tiantsai Lin Professor of Electrical Engineering at Harvard's School of Engineering and Applied Sciences. He received his Diploma (1997) from University of Belgrade (Republic of Serbia) and his MS (1998) and PhD (2003) degrees from California Institute of Technology, all in electrical engineering. His recent research interests include optical nanocavities, diamond nanophotonics and quantum optics, nanoscale optomechanics, and cavity-based bio-chemical sensing. He is recipient of NSF CAREER Award in 2009, and Alfred P. Sloan Fellowship in 2010.

1.1 Challenges in diamond fabrication and material synthesis Due to difficulties associated with the fabrication of nanoscale optical devices in diamond, early approaches to enhance the NV center–photon interaction had mostly relied on hybrid platforms that combine diamond nanocrystals [15] and external optical devices fabricated in non-diamond materials [16, 17]. However, the optical and spin properties of single NV centers found in nanocrystals tend to be inferior to those in bulk diamond and device fabrication lacks scalability. In particular, severe spectral diffusion of the ZPL and its broad linewidths, even at low temperature [18], have limited the applications of diamond nanocrystals.

An enticing approach is to fabricate optical devices directly in diamond and embed individual color centers inside them. However, the realization of such a monolithic system is met with a set of material challenges, namely the difficulty of growing high-quality single crystal diamond films on sacrificial or low index substrates, and the physical and chemical resilience of the material. Ion slicing [19] has been used to realize thin diamond slabs, but damage introduced into the diamond during the process has prevented applications in quantum science. However, recent techniques based on the regrowth of single crystalline material on sliced membranes [20, 21] showed promising

results. An alternative technique used to sculpt optical devices directly in diamond is based on focused ion-beam (FIB) milling [22–25]. Despite the versatility of the method, the resulting devices are prone to damage due to the implantation of gallium ions, although recent experiments indicate that it is possible to minimize this damage using post-processing techniques [26]. FIB can also be used to generate devices in which the NV center is located far away from the processed surface, such as solid-immersion lenses (SILs) [27]. Nonetheless, FIB-fabricated devices are one of a kind and the fabrication process is slow. Therefore, this approach is likely not suitable for the realization of nanoscale optical devices and their large scale integration.

Recent advances in conventional top-down fabrication techniques in diamond allow for three-dimensional [28, 29] and planar [26, 30–32] nanoscale diamond structures to be made with scalability and high yield. This approach involves the patterning of an etch mask using electron beam lithography (EBL) and subsequent reactive-ion etching (RIE) of diamond material in an oxygen-based environment [28]. Thousands of devices can be realized in parallel this way, which suggests that the procedure can eventually enable the construction of chip-scale quantum networks. Additionally, techniques to integrate and deterministically position color centers into dry etched diamond devices via ion implantation are well-established [33].

Device throughput is an important consideration for diamond nanofabrication and greatly depends on the density and distribution of NV centers in the diamond substrate. In type Ib diamond (Element Six, <200 ppm N content), the NV center density is quite high, but varies from chip to chip as well as within the chip. In type IIa mechanical grade CVD diamonds (Element Six, <1 ppm N content), the NV center density is usually too high for single NV centers to be resolved, while it is very low in ultrapure electronic grade CVD diamond (Element Six, <5 ppb N content) to the extent that NV centers are hard to find. However, in the latter case NV centers are of high quality and have ZPL linewidths down to ~20 MHz in resonant absorption [10]. Nonetheless, the randomness in the density and position of natural NV centers makes their integration in optical devices challenging when precise positioning at a mode maximum is required. Implantation of nitrogen ions (usually ^{15}N to distinguish from naturally occurring ^{14}N via the hyperfine splitting signature [2]) offers some control over the depth of NV centers (to the accuracy of the ion straggle) in the crystal by way of the ion energy. The ion dosage and annealing conditions can further increase the probability of proper integration of NV centers to devices by providing some degree of density control.

1.2 NV–photon interaction inside an optical cavity Due to the strong electron phonon coupling that leads to a prominent PSB emission, only ~5% of the overall radiative NV emission goes into the ZPL. This limits the ZPL photon rate to ~1000 counts per second (CPS), in a typical confocal microscope, which in turn significantly limits the applications in quantum science and technology that rely on high rates of indistinguishable photons (e.g., realization of quantum repeaters). This situation can be significantly improved by embedding NV centers inside optical devices which fall in one of two categories:

(1) Non-resonant geometries, like diamond nanowires [28, 29] and solid immersion lenses [27], that overcome total internal reflection (TIR) at the diamond–air interface, can be used to significantly improve the photon collection efficiency without affecting the radiative emission rate of the NV center.
(2) Resonant optical structures, both dielectric and metallic [34], can be used to increase the emission rate of the NV center via the Purcell effect [35]. For applications in quantum science and technology, high-quality factor optical resonators with sharp optical resonances are of particular interest: when their resonance is matched to the NV center's ZPL, selective enhancement of the ZPL emission over the PSB emission can be achieved.

The photon–NV center interaction can be described in terms of the coupling rate g between the emitter and the cavity field, the cavity decay rate κ and the spontaneous emission rate γ. Depending on the relative magnitude of these rates, two different regimes are possible: (i) the weak coupling regime, characterized by $g^2 > \kappa \cdot \gamma$, and (ii) the strong coupling regime, where $g >> \kappa,\ \gamma$. The weak coupling regime (Purcell regime) is of interest in applications that require a large number of ZPL-single photons, including single photon transistor/photon blockade experiments [36, 37], various interference and entanglement scenarios [38–41], or efficient read-out from quantum registers [42, 43]. In this limit, the Purcell factor, F_P, is often used as a figure of merit for spontaneous emission rate enhancement. For an emitter placed at the cavity's field maximum with optimum polarization, F_P is defined as

$$F_P = \frac{g^2}{\gamma\kappa} = \frac{3}{4\pi^2}\left(\frac{\lambda}{n}\right)^3 \frac{Q}{V} > 1. \quad (1)$$

Here, Q represents the quality (Q-) factor that describes the resonator's ability to store photons and the mode volume V is the inverse normalized energy density of the resonator mode. For an NV center, up to 5% of light is emitted into the ZPL. Therefore, a Purcell factor of 20 results in equal emission rates into the ZPL and the PSB and the emitter–cavity system enters the weak coupling regime. This F_P can be achieved with a Q-factor of ~260 and a mode volume of $1(\lambda/n_{\mathrm{diam}})^3$. These parameters can be obtained in photonic crystal cavities (PhCs), assuming that the emitter is optimally coupled to the cavity mode. In addition, the ZPL is usually not lifetime-limited and is broadened by charge fluctuations around the NV center, thereby limiting the feasibility of using the NV center as a source of indistinguishable photons. However, recent advances in resonant absorption techniques might circumvent the issue of spectral instability [44].

In the strong coupling limit, coherent exchange of energy between the NV center and the cavity field exists, and the system undergoes Rabi oscillations between the split dressed states [46]. Strong coupling could enable a full spectral control of the NV center's ZPL emission, as well as extraction of emitted photons into a well defined cavity/waveguide mode. Furthermore, this limit of light–matter interaction is of interest for deterministic, on-demand, single photon sources [47]. While Rabi oscillations have been observed with other solid-state systems [48], this regime of operation is challenging to achieve with NV centers due to the lack of high-Q all-diamond optical resonators ($Q \sim 10^5$), as well as stable NV centers embedded inside optical nanostructures. For example, compared to quantum dot-cavity systems [45], a NV center–diamond cavity system needs to have one order of magnitude larger cavity Q-factor to achieve a comparable lifetime change. This, combined with immature fabrication techniques for diamond, makes the realization of quantum optical devices based on diamond very challenging.

1.3 Article outline In this article, we describe our efforts to generate non-resonant diamond structures, as well as resonant structures in the weakly coupled limit. First, single NV centers coupled to a waveguide mode of a diamond nanowire are discussed as a high photon collection efficiency platform (Fig. 2a). The second geometry considered here consists of a diamond nanopost embedded in silver. This nanocavity takes advantage of the ultra-small mode volume typical of metallic nanodevices to increase the radiative emission rate (Fig. 2b) over a wide wavelength range. The third device described consists of a ring resonator coupled to an optical waveguide (Fig. 2c) – a building block for future on-chip quantum networks. On-chip single-photon routing using this device is discussed as well.

2 Diamond nanowires for high photon collection efficiency

To achieve efficient extraction of single photons from an NV center, we first considered a nanowire structure made in bulk single crystal diamond (Fig. 2a) [28, 29]. The nanowire has a diameter of 200 nm and height of 2 μm. Whereas the collection from a single NV center deeply embedded in a bulk diamond suffers tremendously from TIR at the diamond air interface [28], the nanowire provides a waveguide mode that an enclosed NV center can couple to and thus allows for efficient photon exchange between the optical apparatus and the emitter. Using 3D finite-difference time-domain (FDTD) modeling of a dipole emitter in the center of a nanowire, and averaging over the wavelengths associated with the NV center's emission as well as its polarization ((100) diamond crystal orientation is assumed), we estimated that more than 80% of emitted photons are coupled to the fundamental waveguide mode of the wire, 50% of which are emitted upwards, towards the collection optics [28]. Taking into account the reflection (approximately 10%) at the top nanowire facet, as well as the acceptance angle of a microscope objective with 0.95 N.A., we estimated that more than >30% of the total emitted photons can be collected. This is an order of magnitude improvement over the estimated collection efficiency of NV center in the bulk diamond crystal. Similar count rates have been predicted and measured with SILs, which also enhance photon collection efficiency by overcoming TIR [27].

To confirm our predictions in experiment, diamond nanowires have been fabricated in both synthetic type Ib HPHT (Element Six) and CVD grown type IIa electronic grade diamonds. These samples respectively contain naturally occurring NV centers, created during the diamond synthesis process [29], and NV centers created via ion implantation [33]. The fabrication procedure, illustrated in Fig. 3a, starts with cleaning the diamonds in a boiling 1:1:1 sulfuric:nitric:perchloric acid mixture. Next, EBL is used to define the etch mask in electron-beam sensitive spin-on-glass (HSQ). The mask is then transferred into diamond using an inductively coupled plasma (ICP) reactive ion etching (RIE) with an oxygen-based gas chemistry, and the remaining etch mask is subsequently removed in hydrofluoric (HF) acid. Finally, the sample with fabricated nanowires is cleaned again in a boiling 1:1:1 sulfuric:nitric:perchloric acid mixture in order to reduce the background emission during the optical characterization.

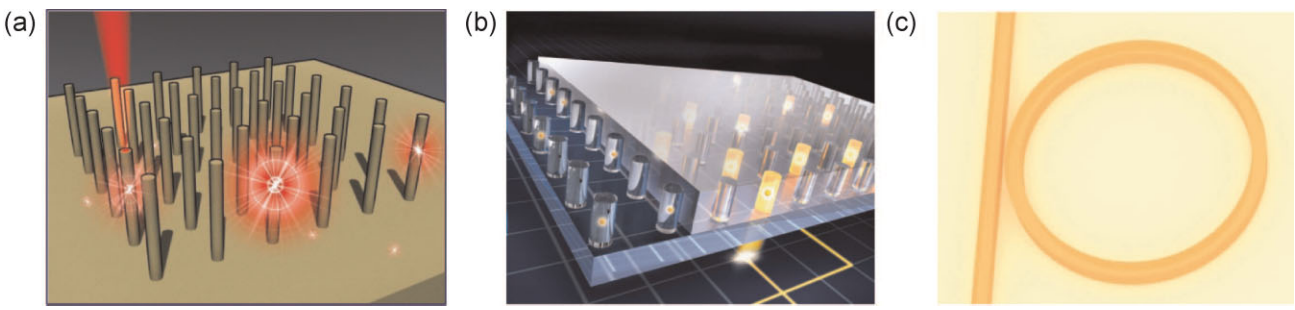

Figure 2 (online color at: www.pss-a.com) Schematics of diamond devices discussed in this article. (a) Diamond nanowires containing single NV centers that provide a high capture of single photon flux. (b) Diamond silver apertures offer Purcell enhancement of the NV center's emission. In a dream quantum network, these silver-capped nanoposts can be envisioned as individual nodes that communicate via single photons that are routed either on- or off-chip. (c) Waveguide coupled diamond ring resonator.

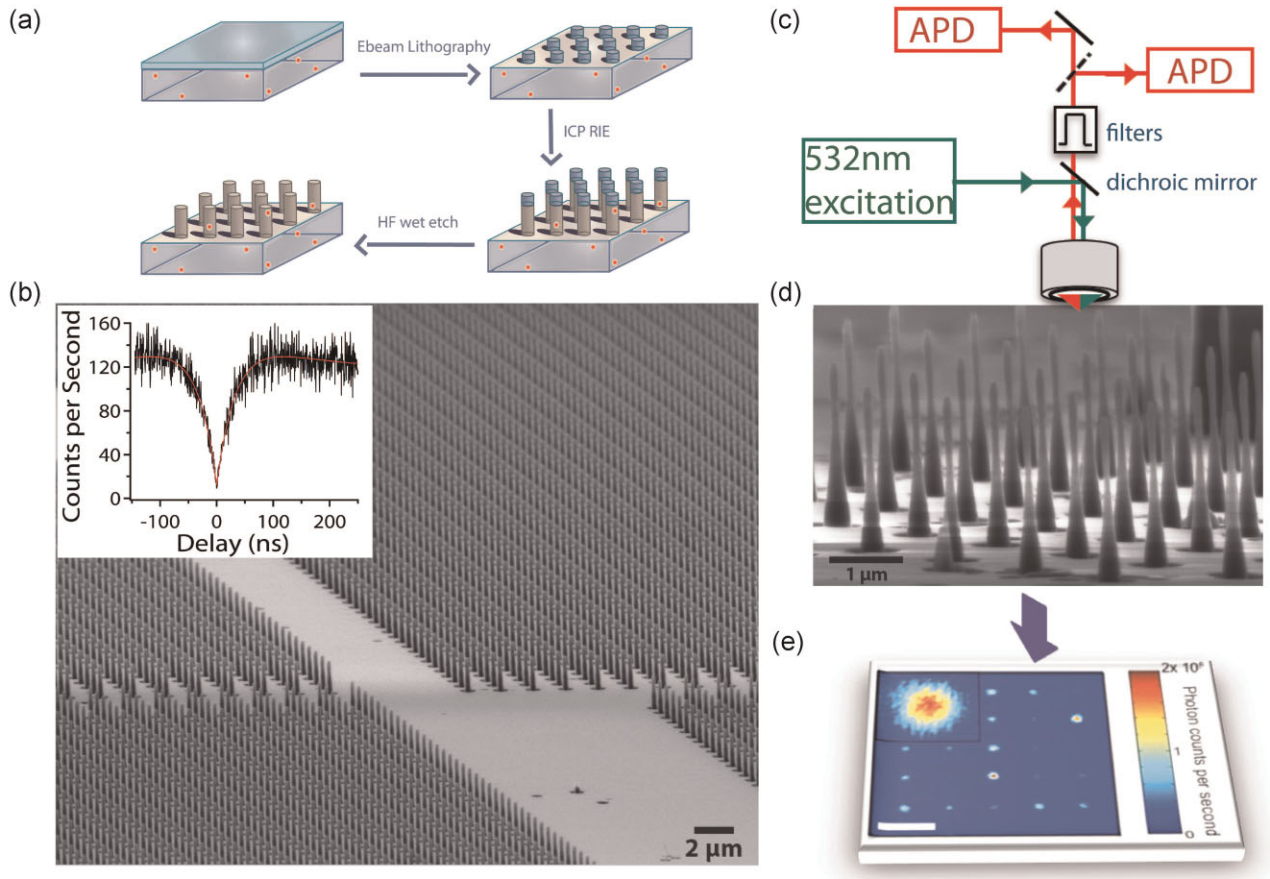

Figure 3 (online color at: www.pss-a.com) Efficient and scalable single photon sources based on diamond nanowires: (a) Fabrication schematic shows spin-on-glass resist deposition, definition of an etch mask using e-beam lithography, transfer of the mask into the diamond via an oxygen RIE step and removal of remaining mask using HF. (b) SEM image of arrays of 2 μm spaced diamond nanowires with 2 μm height and 200 nm diameter. Inset: A second-order correlation function shows a pronounced dip at zero delay indicative of single photon emission for an NV center in a diamond nanowire [33]. (c) A schematic of a confocal microscope setup used to characterize nanowires (d and e). For visualization a (graphically rotated) confocal scan of diamond nanowires is shown in (e).

A scanning electron microscope (SEM) image of an array of fabricated devices is presented in Fig. 3b.

To characterize our devices, a confocal microscope (Fig. 3c) with a 0.95 N.A. air objective is used, resulting in a collection half-angle of 72°. This allows for ideal isolation of a single photon emitter by exciting and collecting emitted photons from a small focal volume (0.25–0.5 μm^3). Such a configuration is suitable for characterizing NV centers in a bulk substrate, as well as in nanowires, and allows for fair comparison between the two geometries. The devices are mounted on a scanning piezo-stage, and a green laser (532 nm) is used to excite the devices. Emission from the NV centers is transmitted through the dichroic mirror, then filtered with a long-pass filter (630 nm) to remove both the excitation light and diamond Raman signal, and finally detected using avalanche photo-diodes (APD) [29]. This allows us to obtain the luminescence image of our sample (Fig. 3e). We note that all measurements of optical devices discussed here have been performed at room temperature.

The emission characteristics of single NV centers embedded in the bulk are compared to those in nanowires. In both cases the presence of a single emitter can be inferred by measuring its second order photon correlation function using the Hanbury Brown–Twiss (HBT) configuration [50]. In the measurement, the photon stream is divided using a beamsplitter (fiber beam splitter in this case), directed to two APDs (Fig. 3c), and the delay between the arrival time of photons is recorded. The finite lifetime of the NV center results in the time delay between photon emission events. Therefore, within one emission lifetime, only one photon can be present in the stream, and only one of the APDs can register photon arrival. Therefore, the intensity correlation function, defined as

$$g^{(2)}(\tau) = \frac{\langle I(\tau + t)I(t)\rangle}{\langle I(t)\rangle^2}$$

where τ is the delay time, is 0 for a perfect single photon flux at $\tau = 0$ (called photon antibunching). Residual background that impinges on the APDs results in $g^{(2)}(0) > 0$ and a true single photon source has $g^{(2)}(0) < 0.5$ as upper bound in the absence of an additional emitter [51]. The width of the dip at

zero delay carries information on the emitter's lifetime and provides a way to measure the lifetime without a pulsed laser source for pump powers below saturation [29]. Away from the dip the photon statistics are Poissonian and result in $g^{(2)}(\tau) = 1$. However, a long-lived intermediate shelving state of the NV center gives rise to $g^{(2)}(\tau) > 1$ in the vicinity of the dip under high pump powers, a phenomenon called bunching [5]. The inset of Fig. 3b shows the pronounced signature of a single photon correlation for an NV center in a nanowire below saturation pump power. Furthermore, lifetimes of single NV centers in nanowires have been extracted from the $g^{(2)}(\tau)$ statistics as well as by pulsed excitation and resulted in 14 ns for both natural as well as implanted NV centers compared to 11 ns in the bulk material [29, 33] and 25 ns in nanocrystals [15].

The overall performance of single NV centers is appraised in their saturation behavior and is statistically compared to that in bulk. Intrinsically, a quantum emitter's emission intensity I levels off after a certain pump level P_{sat} according to $I(P) = \frac{I_{\mathrm{sat}}}{P_{\mathrm{sat}}/P+1}$ [5], where I_{sat} and P are the saturated emission intensity and pump power, respectively. Figure 4 shows saturation intensity levels versus saturation pump powers for several single emitters in nanowires compared to bulk. The nanowire efficiently funnels light to- and from the NV center, resulting in a tenfold improvement in saturation count level at one-tenth of the saturation pump power required in the bulk. The enhancements in excitation and extraction confirm the predictions from FDTD modeling.

Room temperature applications such as magnetometry and near-field sensing can potentially benefit greatly from the brightness of the nanowire geometry. For example, the nanowire antenna effect has been employed to realize a scanning near field and magnetic field sensor [49]. The nanowire is made on a diamond cantilever carved from a thin film diamond slab (50 μm) in a deep dry etch and optical characterization is performed from the cantilever side which is advantageous in terms of collection efficiency (Fig. 5). Here, a magnetic field sensitivity of 56 $\frac{nT}{\sqrt{\mathrm{Hz}}}$ was established for 10 nm deep implanted NV centers at the tip revealing long

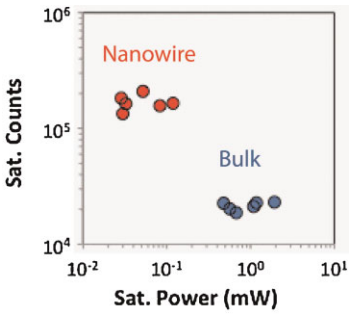

Figure 4 (online color at: www.pss-a.com) Comparison of saturation parameters of the emitter in bulk diamond versus diamond nanowire. The coupling between the emitter and the waveguide mode of the nanowire provides a tenfold improvement in the excitation and photon collection efficiencies [29].

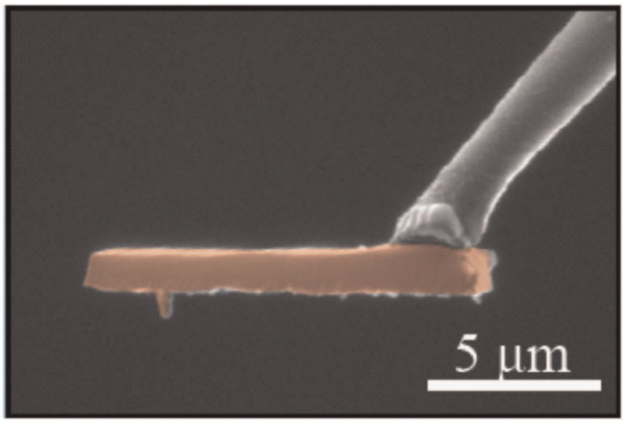

Figure 5 (online color at: www.pss-a.com) An all-diamond magnetometer and near-field sensor based on a diamond nanowire on a diamond cantilever (as indicated by red-colored parts) which itself is attached to an AFM tip. A shallow implanted NV center at the tip of a nanowire is used as a sensitive sensor to image magnetic fields. Figure adapted from [49], with courtesy of Maletinsky.

spin coherence times up to 75 μs. The NV center at the tip can also be used as optical near-field sensor and a spatial resolution of down to 20 nm has been observed.

3 Diamond–silver apertures for broadband enhancement of spontaneous emission rate A complementary approach to improving the single photon yield is to enhance the photon production rate and control the NV center's emission behavior via the Purcell effect, by coupling the color center to a host cavity. Metallic nanocavities [52, 53], are attractive in this regard since they provide strong localization of optical modes with fairly broad bandwidths [54–56]. An interacting emitter then experiences varying degrees of modification in its spontaneous emission rate, depending on the overlap in its position, spectrum, and polarization with those of the cavity system (Section 1.2). The combination of top-down nanofabrication and ion implantation makes it possible to engineer the emitter–cavity interaction in a diamond–plasmon system for many devices in parallel [34]. Subwavelength metallic apertures containing individual color centers can be realized by fabricating arrays of diamond nanoposts in a single crystal diamond substrate that has been implanted with a blanket layer of NV centers (Fig. 6a). The depth and density of defects can be controlled by the implantation energy and dosage, respectively, to ensure that a high fraction of diamond nanoposts contain single NV centers. The diamond nanoposts are finally embedded in a silver (Ag) film and optically addressed through the bulk diamond crystal. The resonances supported by the diamond–plasmon cavities can be tailored to overlap with the NV center emission by changing the post radius as shown by the modeling presented in Fig. 6b. For example, a peak enhancement of 30 can be achieved in the optimized geometry (with aperture radii = 50 nm and height = 180 nm) when the emitter is placed at the field maximum.

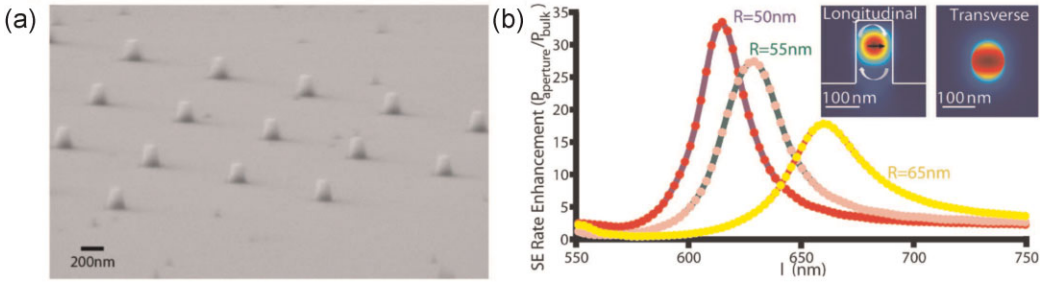

Figure 6 (online color at: www.pss-a.com) Resonators for broadband enhancement of single photon emission. (a) SEM image of an array of bare diamond nanoposts (without silver) containing single implanted color centers. In order to increase the light–matter interaction, posts are embedded in a thick silver layer, as illustrated in Fig. 2b. (b) Simulated spontaneous emission rate enhancement of the diamond–silver aperture (180 nm tall and with an NV center implanted at the center) as a function of wavelength, for three different aperture radii. Insets show the longitudinal and transverse profiles of the electric field distribution of the cavity mode.

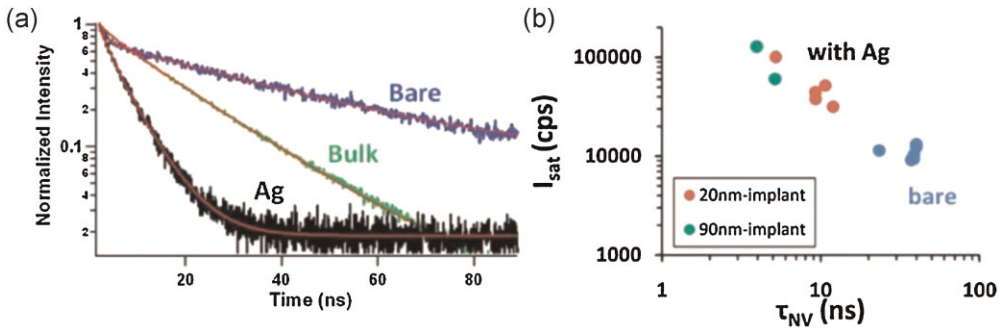

Figure 7 (online color at: www.pss-a.com) Performance of NV centers embedded in plasmonic posts. (a) Normalized fluorescence decay traces for a single NV center implanted 20 nm-deep in a diamond nanopost (with $r = 65$ nm), before (bare) and after silver deposition (Ag), as well as for an ensemble of NV centers in the bulk region. Fits to a multi-exponential model, shown in red, yield time constants for fast-decaying background fluorescence (<2 ns) as well as a slower NV center photoluminescence (bare: 37.17 ± 0.7 ns; silver-embedded: 5.65 ± 0.08 ns; bulk: 16.7 ± 0.08 ns). (b) Scatter plot of saturation intensity as a function of fluorescence lifetime for the bare and silver-capped devices at different implantation depths. The general trend indicates a direct correspondence between the decrease in emitter lifetimes by the plasmonic cavity effect and enhancement in count rates.

The shallow implanted nanostructures have been studied before and after Ag deposition. The NV center's emission is quenched in the bare posts (without silver present) leading to long lifetimes of up to 47 ns. The trend of longer lifetimes is attributed to the vicinity to the surface in the nanoposts (shallow NV centers in unstructured material results in a 17 ns lifetime) and a reduced density of states for the NV center's radiative transition [34]. Time-resolved photoluminescence measurements on diamond nanoposts after Ag deposition indicate that coupling to the plasmonic cavity has resulted in shortening of the emitter lifetime for single NV centers (Fig. 7a). Lifetimes as short as 2.4 ns are observed in the 90 nm implant sample, corresponding to more than a sixfold enhancement in spontaneous emission rate in comparison to the bulk value. The enhancements in the spontaneous emission rate are accompanied by comparable increases in the single photon count rate, which is confirmed by saturation measurements (Fig. 7b).

The presence of NV centers in plasmonic cavities have been also confirmed via their microwave fingerprint in optically detected electron spin resonance (ESR) studies. The characteristic signature is a fluorescence decrease at a microwave frequency of 2.87 GHz that corresponds to the zero-field ground-state splitting between the $m_s = 0$ and $m_s = \pm 1$ states (Fig. 8). Optical excitation from the $m_s = \pm 1$ state couples more strongly to the long-lived singlet shelving state and undergoes fewer fluorescence cycles before decaying to the ground state. Hence, it fluoresces 20–40%

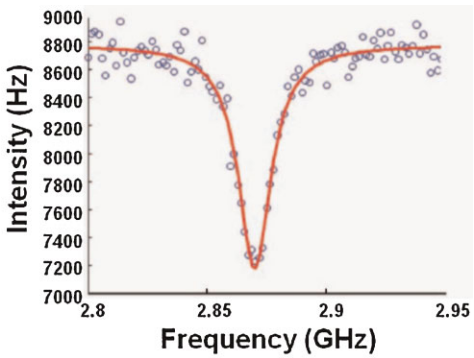

Figure 8 (online color at: www.pss-a.com) Electron spin resonance (ESR) signature of an NV center in a diamond nanopost embedded in silver at 2.87 GHz.

less [4, 57]. From the contrast in the ESR dip, one can deduce the average spin polarization populations. Furthermore, ESR techniques allow for electron spin quantum state read-out [10]. Single-shot read-out measurements have been achieved on an NV center's nuclear spin [58] as well as on a multi quantum bit register consisting of an NV center and nearby nitrogen atoms [59].

4 Diamond ring resonators and on-chip diamond photonic networks The devices discussed above are particularly suitable for applications where single photons are extracted from the chip and coupled to free-space optics. However, for many applications, including the realization of scalable quantum networks, it is of interest to use photons to transmit information and perform computation throughout the chip. There is therefore a need to develop a fully integrated diamond photonic platform. To achieve this goal, we developed techniques to generate a diamond-on-insulator platform containing an optically thin diamond device layer. A type Ib diamond with randomly distributed NV centers has been used for this purpose. First, a high-quality single-crystal thin slabs $<50\,\mu m$ is placed on a low-index substrate, such as silica, and thinned, using ICP RIE, to form an optically thin diamond waveguide slab. Next, the film is bonded to a silica on silicon substrate, and EBL is used to define the etch mask in a spin-on-glass resist. Then, a second ICP RIE step is used to transfer the mask into the thinned diamond slab. The main advantage of the approach lies in the high crystal quality that can be maintained for the optical devices. This versatile approach allows for a variety of nanophotonic devices and systems to be made in diamond, including ring resonators [30, 31] and PhCs [32, 60]. We note, however, that the handling of thin diamond substrates ($<1\,\mu m$ thickness) and wedging of the diamond films can limit the device throughput.

A SEM image of one of our devices is shown in Fig. 9a. It consists of a diamond ring resonator coupled to a diamond waveguide with second order gratings defined at its ends for efficient in- and outcoupling of light. A ring diameter of $5\,\mu m$ has been chosen as a trade-off between having small mode volume $(28(\lambda/n_{diam})^3)$ and large quality factor. A ring-waveguide separation of 100 nm and a cross-section of approximately 250 nm × 250 nm, respectively ensure single mode operation as well as efficient ring–waveguide coupling. Optical characterization was performed in a confocal microscope that has two collection channels. One channel collects photons at the excitation spot whereas the independent second arm collects photons from a different spot. For initial characterization, white light is directed towards one coupling grating through the first pump/collection channel

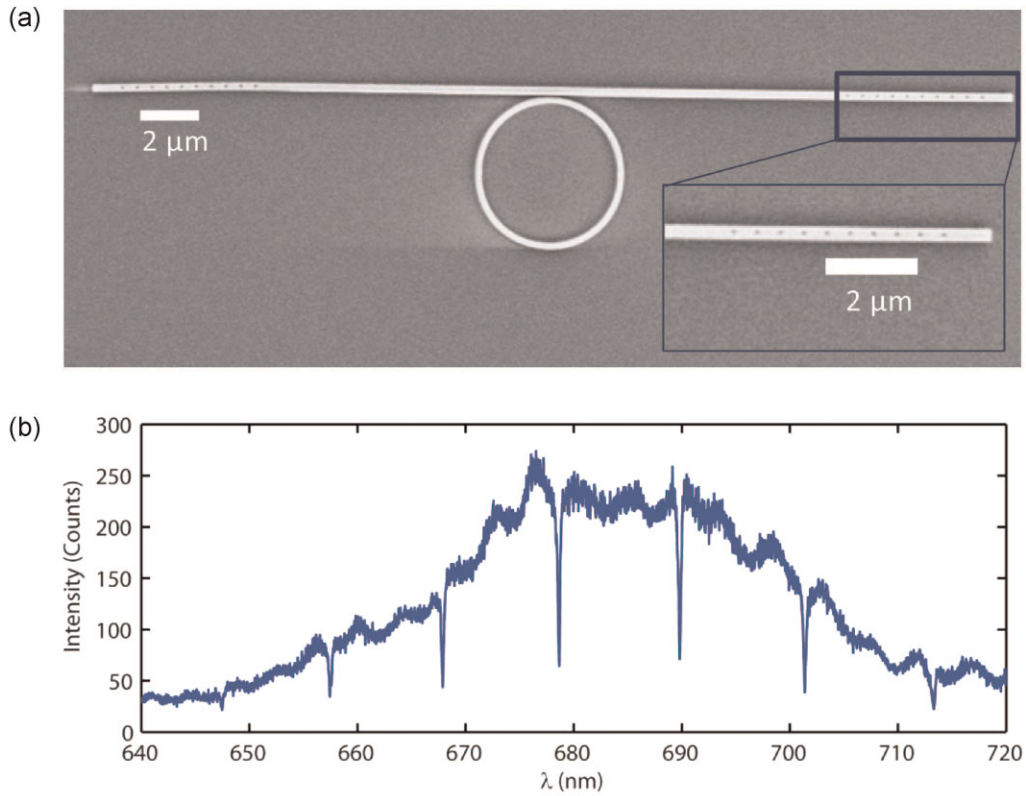

Figure 9 (online color at: www.pss-a.com) Integrated diamond ring resonators on silica. (a) SEM image of a 5 μm diameter diamond ring resonator on a SiO_2/Si chip coupled to a diamond waveguide containing outcoupling gratings that consist of periodic holes. Diamond ring resonators were made from thin single crystal diamond slabs for optical characterization in the visible wavelength regime. (b) White light excitation at one end of the waveguide is used to measure the quality factors of the ring resonators via extraction of transmitted light at the other end of the waveguide. Q-factors as high as 3200 were measured for the device shown [31].

while transmitted light at the other coupling grating is collected by the second collection channel. Spectra obtained in this fashion reveal periodic resonator modes with linewidths corresponding to Q-factors up to 3200 (Fig. 9b).

After a device is identified in transmission studies, single NV centers in the ring are evaluated. Here, the pump laser (as well as the first collection arm) is placed at the NV center (indicated by the red circle in Fig. 10a) and the second arm is placed either at the NV center or at the end of the waveguides (indicated by the yellow circle in Fig. 10a). Second order autocorrelation measurements are performed to confirm single photon emission while collecting only above the NV center. Then, cross-correlation between the first collection arm at the NV center and the second one at the end of the waveguide is performed to reveal pronounced anti-bunching

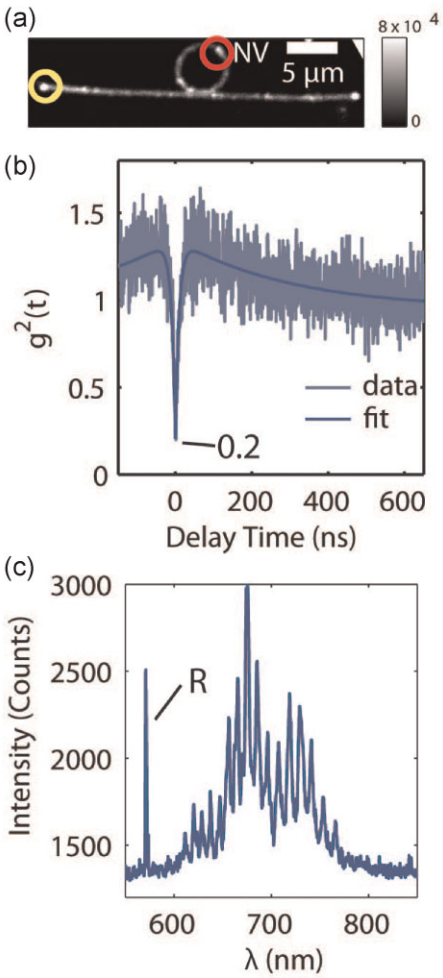

Figure 10 (online color at: www.pss-a.com) Single photon routing on-chip. (a) A confocal scan reveals single NV centers coupled to the ring resonator. The confocal microscope used here allows for having different pump and collection positions. (b) Cross-correlation between photons collected at the pump position (at the NV center location) and at the end of the waveguide shows a pronounced dip at zero time-delay indicating on-chip single photon routing. (c) The spectrum at the outcoupling grating features resonances imprinted on the NV center's spectrum as expected for single photon routing [60].

at zero delay with a comparable contrast to the previous g^2 study (Fig. 10b). The low background level is remarkable for a type Ib diamond and is due to the small amount of diamond material left after processing. More importantly, the cross-correlated $g^{(2)}$ measurement unambiguously confirms the routing of single photons on-chip. The spectrum at the out-coupling grating shows periodic resonator modes superimposed on the NV center's emission (Fig. 10c). The Q-factors inferred from the photoluminescence spectrum match those obtained in transmission measurements. Overall, 10% of the NV center's free-space emission was collected at the end of the waveguides based on saturation studies [31].

The geometry presented here is a new form of diamond-on-insulator platform that provides versatility in applications as well as scalability, while maintaining the high single crystal diamond quality as inferred from Raman spectra [31]. An optical network consisting of quantum nodes (NV centers coupled to cavities) connected by single photon channels (optical waveguides) could enable scalable quantum networks that allow for quantum information to be stored, manipulated and transferred on-chip. The method presented here could lead to more sophisticated integrated quantum networks used for photon entanglement of distant NV centers coupled to separate devices on chip.

5 Summary and outlook In the past five years, diamond research has evolved from working with color centers in bulk material or nanocrystals to their controlled integration in nanodevices. However, while progress in the field has been tremendous, there are outstanding challenges that still need to be addressed.

5.1 Implantation of NV centers A good NV center implantation yield was observed in the case of shallow implanted NV centers in nanowires where up to 30% of nanowires contained single NV centers [49]. An outstanding challenge that needs to be resolved before advancing to more involved quantum optics studies of NV centers embedded in nanophotonic devices, is obtaining stable, narrow-ZPL NV centers at low temperature.

5.2 Nanowires An order of magnitude more efficient exchange of pump photons and emitted single photons has been obtained in form of a NV center-coupled nanowire geometry ($\approx 2 \times 10^5$ CPS) compared to an NV center in bulk ($\approx 2 \times 10^4$ CPS). Its single photon count level is also higher compared to typical nanocrystals that emit in the mid 10^4 CPS range [15]. We note, however, that count rates of $\approx 1 \times 10^5$ CPS have been observed for nanocrystals placed at the end of an optical fiber [61]. Since the nanowire provides directional emission, it could be integrated with a simple lensed fiber. Overall, the increased collection efficiency of the nanowire geometry facilitates optical studies of the NV center. Furthermore, the scalability of the fabrication approach can enable entanglement measurements that require a large number of devices to provide a high probability of identical ZPLs, as well as high single photon

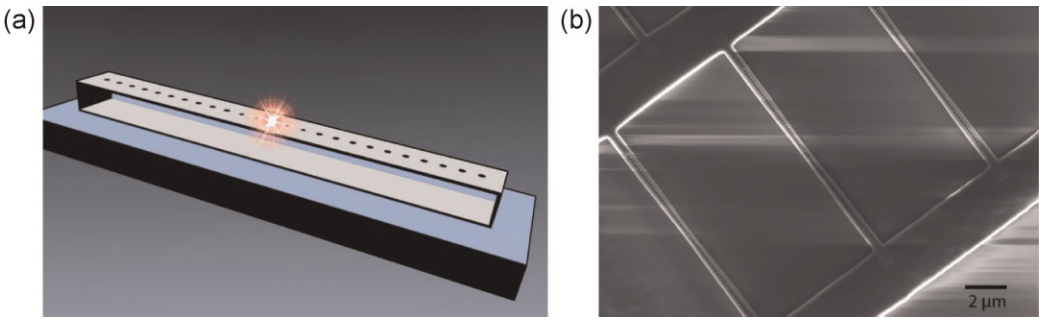

Figure 11 (online color at: www.pss-a.com) Photonic crystal nanobeam cavities in diamond. (a) Schematic of an NV center coupled to a photonic crystal nanobeam, and a (b) top-view SEM image of fabricated diamond photonic crystal nanobeams on silica substrate.

flux. For these applications, low temperature operation is required in order to resolve the ZPL of the NV centers. However, low-temperature studies of implanted NV centers in diamond nanowires (as well as diamond nanocrystals) have not yet offered photo-stability combined with narrow ZPLs. The spectral instability might be attributed to surface effects originating from the etch procedure, surface termination, and surface traps. These can result in NV center charge state conversion and a fluctuating charge environment which causes severe spectral diffusion of the ZPL.

5.3 Plasmonic resonators A broadband enhancement of spontaneous emission has lead to a sixfold increase in the emission rate of NV centers placed in plasmonic ultrasmall mode volume resonators. However, photon collection efficiency in the system remains limited by losses to surface plasmons as well as TIR at the collection (bottom) facet of the diamond substrate, so that only about 5% of the total emitted photons are collected. A modified geometry with thinner silver layer that allows for photons to be collected from the top surface of the sample should result in even larger photon collection efficiency [56]. Future developments will also include the addition of gratings (e.g. bull's eye pattern) to coherently scatter surface plasmons into the critical cone thus improving the collection efficiency [62]. Potential applications of the diamond–plasmon system include improved optical readout for NV center-based nanoscale magnetometry [49, 63] and faster rates for quantum communication and computation processes based on either spin or photonic qubits (Fig. 2b). However, practical implementation of the device would require a sufficiently long spin coherence time as well as stable emission lines at low temperature for the shallow-implanted NV centers, which remain to be confirmed in experiments.

5.4 Planar integration Integrated diamond photonics has recently emerged as a promising platform for quantum science. Photonic crystal and ring cavities, as well as optical waveguides and gratings have been demonstrated using this approach. Furthermore, on-chip single photon routing has been achieved for NV centers in planar ring resonators coupled to waveguides. Quality factors of these resonators are likely limited by surface roughness and possibly absorption losses in the visible wavelength range. Future experiments will focus on improving the performance of diamond ring resonators as well as investigation of NV centers coupled to PhCs (Fig. 11). Since PhCs provide a much higher Q/V ratio compared to the ring resonators, much stronger light–matter interaction between the NV center and the cavity field may be achieved. Meanwhile, the likelihood of having an NV center coupled to the cavity region is reduced, due to the smaller cavity size. Moreover, surface effects such as surface traps and functionalization may have greater impact on implanted NV centers that are located in close proximity to the surface. Therefore, further studies and developments of surface treatments and annealing protocols are needed to enable wide-spread applications of diamond PhCs. So far, Purcell enhancement of around 70 has been reported [32] which is up to six times higher than what has been achieved with ring resonators [30]. Finally, novel techniques, based on bulk nanomachining of diamond [64] can further facilitate the developments in the field of quantum diamond photonics.

Acknowledgements We would like to acknowledge all authors of the papers discussed here, especially Y. Zhang, Q. Quan, M. Grinolds, S. Hong, P. Maletinsky, A. Kubanek, M. Khan, J. Maze, M. McCutcheon, A. Yacoby, and P. Hemmer. We thank Florian Huber for help with the preparation of cartoons in Figs. 2a and 7. Devices were fabricated in the Center for Nanoscale Systems (CNS) at Harvard. The authors thank Daniel Twitchen and Matthew Markham from Element Six for support with diamond samples. B. H. gratefully acknowledges support from the Harvard Quantum Optics Center (HQOC). This work was supported in part by the Defense Advanced Research Projects Agancy (Quantum Entanglement Science and Technology program), Harvard University's Nanoscale Science and Engineering Center (NSEC), a NSF Nanotechnology and Interdisciplinary Research Team Grant (ECCS-0708905), the Hewlett Packard Foundation, and AFOSR MURI (grant FA9550-09-1-0669-DOD35CAP). M.Lo. acknowledges support from the Sloan Foundation.

References

[1] G. Balasubramanian, P. Neumann, D. Twitchen, M. Markham, R. Kolesov, N. Mizuochi, J. Isoya, J. Achard, J. Beck, J. Tissler, V. Jacques, P. R. Hemmer, F. Jelezko, and J. Wrachtrup, Nature Mater. **8**, 383 (2009).

[2] F. Jelezko and J. Wrachtrup, Phys. Status Solidi A **203**(13), 3207–3225 (2006).
[3] A. M. Zaitsev, Optical Properties of Diamond: A Data Handbook (Springer-Verlag, Berlin, Heidelberg, New York, 2001).
[4] A. Gruber, A. Drabenstedt, C. Tietz, L. Fleury, J. Wrachtrup, and C. von Borczyskowski, Science **276**, 2012 (1997).
[5] C. Kurtsiefer, S. Mayer, P. Zarda, and H. Weinfurter, Phys. Rev. Lett. **85**, 290 (2000).
[6] F. Jelezko, C. Tietz, A. Gruber, I. Popa, A. Nizovtsev, S. Kilin, and J. Wrachtrup, Single Mol. **2**, 255–260 (2001).
[7] G. Balasubramanian, I. Y. Chan, R. Kolesov, M. Al-Hmoud, J. Tisler, C. Shin, C. Kim, A. Wojcik, P. R. Hemmer, A. Krueger, T. Hanke, A. Leitenstorfer, R. Bratschitsch, F. Jelezko, and J. Wrachtrup, Nature **455**(7213), 648–651 (2008).
[8] J. R. Maze, P. L. Stanwix, J. S. Hodges, S. Hong, J. M. Taylor, P. Cappellaro, L. Jiang, M. V. G. Dutt, E. Togan, A. S. Zibrov, A. Yacoby, R. L. Walsworth, and M. D. Lukin, Nature **455**, 644 (2008).
[9] L. I. Childress, Coherent manipulation of single quantum systems in the solid state, PhD thesis, The Department of Physics, Harvard University (2007).
[10] J. Wrachtrup and F. Jelezko, J. Phys.: Condens. Matter **18**, 807–824 (2006).
[11] L. Childress, J. M. Taylor, A. S. Sørensen, and M. D. Lukin, Phys. Rev. Lett. **96**, 070504 (2006).
[12] A. Beveratos, R. Brouri, T. Gacoin, A. Villing, J. P. Poizat, and P. Grangier, Phys. Rev. Lett. **89**, 187901 (2002).
[13] R. P. Mildren, J. E. Butler, and J. R. Rabeau, Opt. Express **16**(23), 18950 (2008).
[14] A. A. Demidovich, A. S. Grabtchikov, V. A. Orlovich, M. B. Danailov, and W. Kiefer, Conf. Dig. Lasers and Electro-Optics Europe (Optical Society of America, Washington DC, 2005) p. 251
[15] A. Beveratos, R. Brouri, T. Gacoin, J. P. Poizat, and P. Grangier, Phys. Rev. A **64**, 061802(R) (2001).
[16] D. Englund, B. Shields, K. Rivoire, F. Hatami, J. Vuckovic, H. Park, and M. D. Lukin, Nano Lett. **10**, 3922 (2010).
[17] T. van der Sar, J. Hagemeier, W. Pfaff, E. C. Heeres, S. M. Thon, H. Kim, P. M. Petroff, T. H. Oosterkamp, D. Bouwmeester, and R. Hanson, Appl. Phys. Lett. **98**, 193103 (2011).
[18] J. Wolters, N. Sadzak, A. W. Schell, T. Schroeder, and O. Benson, arXiv:1206.0852v1 (2012).
[19] P. Olivero, S. Rubanov, P. Reichart, B. C. Gibson, S. T. Huntington, J. Rabeau, A. D. Greentree, J. Salzman, D. Moore, D. N. Jamieson, and S. Prawer, Adv. Mater. **17**, 2427–2430 (2005).
[20] I. Aharonovich, J. C. Lee, A. P. Magyar, B. B. Buckley, C. G. Yale, D. D. Awschalom, and E. L. Hu, Adv. Mater. **24**(10), OP54 (2012).
[21] A. P. Magyar, J. C. Lee, A. M. Limarga, I. Aharonovich, F. Rol, D. R. Clarke, M. Huang, and E. L. Hu, Appl. Phys. Lett. **99**, 081913 (2011).
[22] T. M. Babinec, J. T. Choy, K. J. M. Smith, M. Khan, and M. Loncar, J. Vac. Sci. Technol. B **29**(1), 010601 (2010).
[23] T. Schroeder, F. Gädeke, M. J. Banholzer, and O. Benson, New J. Phys. **13**, 055017 (2011).
[24] I. Bayn, B. Meyler, A. Lahav, J. Salzman, R. Kalish, B. A. Fairchild, S. Prawer, M. Barth, O. Benson, T. Wolf, P. Siyushev, F. Jelezko, and J. Wrachtrup, Diam. Relat. Mater. **20**(7), 937 (2011).
[25] T. Babinec, B. Hausmann, J. Choy, M. Khan, P. Hemmer, and M. Loncar, IEEE Photon. Soc. Newsletter **25**, 13 (2011).
[26] J. Riedrich-Moeller, L. Kipfstuhl, C. Hepp, E. Neu, C. Pauly, F. Muecklich, A. B. M. Wandt, S. Wolff, M. Fischer, S. Gsell, M. Schreck, and C. Becher, Nature Nanotechnol. **7**, 69 (2012).
[27] J. P. Hadden, J. P. Harrison, A. C. Stanley-Clarke, L. Marseglia, Y. L. D. Ho, B. R. Patton, J. L. O'Brien, and J. G. Rarity, Appl. Phys. Lett. **97**, 241901 (2010).
[28] B. J. M. Hausmann, M. Khan, T. Babinec, Y. Zhang, K. Martinick, M. McCutcheon, P. Hemmer, and M. Loncar, Diam. Relat. Mater. **19**, 621 (2010).
[29] T. M. Babinec, B. J. M. Hausmann, M. Khan, Y. Zhang, J. Maze, P. R. Hemmer, and M. Loncar, Nature Nanotechnol. **5**, 195–199 (2010).
[30] A. Faraon, P. E. Barclay, C. Santori, K. M. C. Fu, and R. G. Beausoleil, Nature Photon. **5**, 301–305 (2011).
[31] B. J. M. Hausmann, B. S. Q. Quan, P. Maletinsky, M. McCutcheon, J. T. Choy, T. M. Babinec, A. Kubanek, A. Yacoby, M. D. Lukin, and M. Loncar, Nano Lett. **12**(3), 1578 (2012).
[32] A. Faraon, C. Santori, Z. Huang, V. M. Acosta, and R. G. Beausoleil, Phys. Rev. Lett. **109**, 033604 (2012).
[33] B. J. M. Hausmann, T. M. Babinec, J. T. Choy, J. S. Hodges, S. Hong, I. Bulu, A. Yacoby, M. Lukin, and M. Loncar, New J. Phys. **13**, 045004 (2011).
[34] J. T. Choy, B. J. M. Hausmann, T. M. Babinec, I. Bulu, M. Khan, P. Maletinsky, A. Yacoby, and M. Loncar, Nature Photon. **5**, 738 (2011).
[35] E. M. Purcell, Phys. Rev. **69**, 681 (1946).
[36] D. E. Chang, A. S. Sørensen, E. A. Demler, and M. D. Lukin, Nature Phys. **3**, 807–8812 (2007).
[37] K. M. Birnbaum, R. M. A. Boca, A. D. Boozer, T. E. Northup, and H. J. Kimble, Nature **436**, 87 (2005).
[38] B. B. Blinov, D. L. Moehring, L. M. Duan, and C. Monroe, Nature **428**, 153 (2004).
[39] P. Neumann, N. Mizuochi, F. Rempp, P. Hemmer, H. Watanabe, S. Yamasaki, V. Jacques, T. Gaebel, F. Jelezko, and J. Wrachtrup, Science **320**, 1326 (2008).
[40] E. Togan, Y. Chu, A. S. Trifonov, L. Jiang, J. Maze, L. Childress, M. V. G. Dutt, A. S. Sørensen, P. R. Hemmer, A. S. Zibrov, and M. D. Lukin, Nature **466**, 730–734 (2010).
[41] W. Pfaff, T. H. Taminiau, L. Robledo, H. Bernien, M. L. Markham, D. J. Twitchen, and R. Hanson, arXiv:1206.2031v1 (2012).
[42] M. V. G. Dutt, L. Childress, L. Jiang, E. Togan, J. Maze, F. Jelezko, A. S. Zibrov, P. R. Hemmer, and M. D. Lukin, Science **316**, 1312 (2007).
[43] P. Neumann, R. Kolesov, B. Naydenov, J. Beck, F. Rempp, M. Steiner, V. Jacques, G. Balasubramanian, M. L. Markham, D. J. Twitchen, S. Pezzagna, J. Meijer, J. Twamley, F. Jelezko, and J. Wrachtrup, Nature Phys. **6**, 249 (2010).
[44] P. Siyushev, H. Pinto, A. Gali, F. Jelezko, and J. Wrachtrup, arXiv:1204.4898v1 (2012).
[45] J. Vuckovic and Y. Yamamoto, Appl. Phys. Lett. **82**(15), 2374 (2003).
[46] M. Ducloy and D. Bloch, Quantum Optics of Confined Systems (Kluwer Academic Publishers, Dordrecht, The Netherlands, 1996).

[47] J. McKeever, A. Boca, A. D. Boozer, R. Miller, J. R. Buck, A. Kuzmich, and H. J. Kimble, Science **303**, 1992 (2004).
[48] J. P. Reithmaier, G. Sek, A. Loeffler, C. Hofmann, S. Kuhn, S. Reitzenstein, L. V. Keldysh, V. D. Kulakovskii, T. L. Reinecke, and A. Forchel, Nature **432**, 197 (2004).
[49] P. Maletinsky, S. Hong, M. Grinolds, B. J. M. Hausmann, M. D. Lukin, R. L. Walsworth, M. Loncar, and A. Yacoby, Nature Nanotechnol. **7**, 320 (2012).
[50] R. H. Brown and R. Q. Twiss, Nature **177**, 27–29 (1956).
[51] H. J. Kimble, M. Dagenais, and L. Mandel, Phys. Rev. Lett. **39**, 691 (1977).
[52] T. W. Ebbesen, H. J. Lezec, H. F. Ghaemi, T. Thio, and P. Wolff, Nature **391**, 667 (1998).
[53] N. P. de Leon, B. J. Shields, C. L. Yu, D. Englund, A. V. Akimov, M. D. Lukin, and H. Park, Phys. Rev. Lett. **108**, 226803 (2012).
[54] S. Schietinger, M. Barth, T. Aichele, and O. Benson, Nano Lett. **9**(4), 1694–1698 (2009).
[55] I. S. Maksymov, M. Besbes, J. P. Hugonin, J. Yang, A. Beveratos, I. Sagnes, I. Robert-Philip, and P. Lalanne, Phys. Rev. Lett. **105**, 180502 (2010).
[56] I. Bulu, T. M. Babinec, B. J. M. Hausmann, J. T. Choy, and M. Loncar, Opt. Express **19**, 5269 (2011).
[57] F. Jelezko, I. Popa, A. Gruber, C. Tietz, J. Wrachtrup, A. Nizovtsev, and S. Kilin, Appl. Phys. Lett. **81**(12), 2160 (2002).
[58] P. Neumann, J. Beck, M. Steiner, F. Rempp, H. Fedder, P. R. Hemmer, J. Wrachtrup, and F. Jelezko, Science **329**, 542 (2010).
[59] L. Robledo, L. Childress, H. Bernien, B. Hensen, P. F. A. Alkemade, and R. Hanson, Nature **477**, 574 (2011).
[60] B. J. M. Hausmann, B. Shields, Q. Quan, J. T. Choy, M. W. McCutcheon, P. Maletinsky, T. M. Babinec, Y. Chu, A. Kubanek, A. Yacoby, M. D. Lukin, and M. Loncar, A diamond quantum router of single photons at room temperature, in: MRS Fall meeting, 2011.
[61] T. Schroeder, P. Engel, E. Schmidt, and O. Benson, Opt. Lett. **37**(14), 2901 (2012).
[62] H. J. Lezec, A. Degiron, E. Devaux, R. A. Linke, L. Martin-Moreno, F. J. Garcia-Vidal, and T. W. Ebbesen, Science **297**(5582), 820 (2002).
[63] D. L. Sage, L. M. Pham, N. Bar-Gill, C. Belthangady, M. D. Lukin, A. Yacoby, and R. L. Walsworth, Phys. Rev. B **85**, 121202(R) (2012).
[64] M. Burek, B. Shields, N. P. de Leon, B. Hausmann, Y. Chu, Q. Quan, M. Lukin, and M. Loncar, Angle-etched free-standing photonic crystal nanobeam cavities in single-crystal diamond, in: CLEO/QELS, 2012.

